INSTANTANEOUS VELOCITY VECTOR ESTIMATION USING A SINGLE MIMO RADAR VIA MULTI-BOUNCE SCATTERING

Nishant Mehrotra*, Divyanshu Pandey*, Upamanyu Madhow[†], Yasamin Mostofi[†], and Ashutosh Sabharwal*

*Department of Electrical & Computer Engineering, Rice University, Houston, TX †Department of Electrical & Computer Engineering, University of California, Santa Barbara, CA

ABSTRACT

Multiple-input, multiple-output (MIMO) radars can estimate radial velocities of moving objects, but not their tangential velocities. In this paper, we propose to exploit multi-bounce scattering in the environment to form an effective multi-"look" synthetic aperture and enable estimation of a moving object's entire velocity vector – both tangential and radial velocities. The proposed approach enables instantaneous velocity vector estimation with a single MIMO radar, without additional sensors or assumptions about the object size. The only requirement of our approach is the existence of at least one resolvable multi-bounce path to the object from a static landmark in the environment. The approach is validated both in theory and simulation.

Index Terms— Multipath, MIMO radar, velocity measurement, radar imaging.

1. INTRODUCTION

Multiple-input, multiple-output (MIMO) radars enable high resolution sensing & imaging at low form factors and price points. Conventional MIMO radar algorithms only model single-bounce scattering, wherein signals transmitted by the radar are scattered directly back by objects in the environment: $radar \rightarrow object \rightarrow radar$. However, such models only enable estimating the radial velocities of moving objects, and not tangential velocities. Radial velocity estimates alone can be misleading when objects move tangentially to the radar, and can impact the performance of downstream moving object detection and classification tasks, especially in time-critical applications like autonomous vehicle navigation.

In this work, we propose to exploit paths that scatter more than once in the environment (*multi-bounce*) to estimate the *full velocity vector* – both tangential and radial velocities – of a moving object. The key insight is that the tangential velocity components fall along paths that don't scatter directly back to the radar, but to other objects in the environment. An example scenario is illustrated in Fig. 1, with a MIMO radar tracking a person walking near a building pillar. While the

This work was partially supported by the NSF grant CNS-2215082.

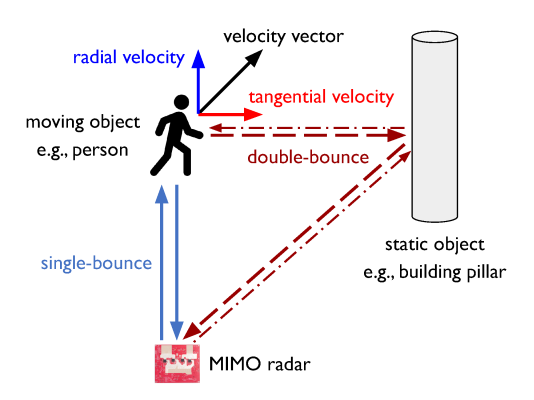


Fig. 1: Velocity vector estimation via multi-bounce.

radial velocity component falls along the single-bounce path: radar \rightarrow person \rightarrow radar, the tangential velocity component falls along double-bounce paths: radar \rightarrow person \rightarrow pillar \rightarrow radar and radar \rightarrow pillar \rightarrow person \rightarrow radar. Hence, both tangential and radial velocities can be estimated by jointly processing the single- and double-bounce paths. The proposed idea can be understood as the velocity vector analogue of multi-"look" synthetic aperture radar, with different multi-bounce paths in the environment providing different "looks" of a given moving object's velocity vector.

Prior Work: To the best of our knowledge, the idea of using multi-bounce for velocity vector estimation is novel and has not appeared previously. Classical approaches to the problem involve tracking targets over multiple frames [1, 2]; however these methods require multiple frames to converge to reliable estimates, and hence can not provide instantaneous velocity vector estimates in every frame. Other works have explored complementary ideas for instantaneous velocity vector estimation with single-bounce models – utilizing multiple cooperative radars [3, 4, 5, 6, 7], fusing measurements from a radar and camera [8], or require extended targets spanning multiple resolution bins [9, 10, 11]. Our proposed approach enables instantaneous velocity vector estimation with a single MIMO radar, without additional sensors or assumptions about the object size. The only requirement of our approach is the existence of ≥ 1 angle-resolvable multi-bounce paths to/from the object due to static landmarks in the environment.

2. PROBLEM FORMULATION

2.1. System Model

Consider the scenario shown in Fig. 1, with a MIMO radar tracking a moving object in the presence of another static object. We model both objects as point targets with 2D location vectors 1 \mathbf{r}_{SB} (moving object) and \mathbf{r}_{DB} (static object) in the range-azimuth plane, neglecting the height of objects. Let \mathbf{v}_{SB} denote the 2D velocity vector of the moving object.

Let T and R denote the number of transmit and receive elements on the radar. The radar transmits P FMCW 2 chirps, of starting frequency f_c & duration T_c , in a time-orthogonal fashion across all T antennas. We assume single-bounce returns from the static object have been measured and cancelled prior to the system's operation (*background subtraction*), reasonable since the static object can be monitored over long durations in the absence of the moving object. After background subtraction, the radar only receives single-bounce and double-bounce paths from the moving object, as shown in Fig. 1, and knows the static object's location $\hat{\mathbf{r}}_{DB}$. The TR \times 1 vector of received signals at the radar (post-matched filtering), in terms of FMCW instantaneous frequency ω and chirp index p, is

$$\mathbf{y}(\omega; \mathbf{p}) = \sigma_{\mathrm{SB}} \left(\mathbf{a}_{\mathrm{RX}} (\theta_{\mathrm{SB}}) \otimes \mathbf{a}_{\mathrm{TX}} (\theta_{\mathrm{SB}}) \right) e^{-j \left[\frac{\omega}{c} \mathbf{d}_{\mathrm{SB}} + 2\pi \mathbf{f}_{\mathrm{D}}^{\mathrm{SB}} \mathbf{p} \mathbf{T}_{\mathrm{c}} \right]} \beta_{\mathrm{SB}}$$
$$+ \sigma_{\mathrm{SB}} \sigma_{\mathrm{DB}} \left(\tilde{\mathbf{a}}_{\mathrm{SB}}^{\mathrm{DB}} \right) e^{-j \left[\frac{\omega}{c} \mathbf{d}_{\mathrm{SB}}^{\mathrm{DB}} + 2\pi \mathbf{f}_{\mathrm{D}}^{\mathrm{DB}} \mathbf{p} \mathbf{T}_{\mathrm{c}} \right]} \beta_{\mathrm{SB}}^{\mathrm{DB}} + \mathbf{n}, \quad (1)$$

where $\tilde{\mathbf{a}}_{\scriptscriptstyle SB}^{\scriptscriptstyle DB} = \mathbf{a}_{\scriptscriptstyle RX}(\theta_{\scriptscriptstyle DB}) \otimes \mathbf{a}_{\scriptscriptstyle TX}(\theta_{\scriptscriptstyle SB}) + \mathbf{a}_{\scriptscriptstyle RX}(\theta_{\scriptscriptstyle SB}) \otimes \mathbf{a}_{\scriptscriptstyle TX}(\theta_{\scriptscriptstyle DB}),$ c denotes the speed of light, and we have assumed the radar's time-bandwidth product is small enough (narrowband) that the objects remain in the same location bins across all P chirps. Variables $\sigma_{\scriptscriptstyle S/DB}$ denote the reflectivities of the single-bounce (moving)/double-bounce (static) objects, and \otimes denotes the Kronecker product. Variables $\mathbf{a}_{\scriptscriptstyle T/RX}(\theta_{\scriptscriptstyle S/DB})$ denote the T \times 1 transmit/R \times 1 receive steering vectors for azimuth angles corresponding to the single/double-bounce object locations. Reflections from the objects result in phase terms proportional to the single-bounce and double-bounce path distances, $\mathbf{d}_{\scriptscriptstyle SB}=2\|\mathbf{r}_{\scriptscriptstyle SB}\|_2$ and $\mathbf{d}_{\scriptscriptstyle SB}^{\scriptscriptstyle DB}=\|\mathbf{r}_{\scriptscriptstyle SB}\|_2+\|\mathbf{r}_{\scriptscriptstyle SB}-\mathbf{r}_{\scriptscriptstyle DB}\|_2+\|\mathbf{r}_{\scriptscriptstyle DB}\|_2$. Variables $\beta_{\scriptscriptstyle SB}=\frac{\alpha_{\scriptscriptstyle TX}}{\|\mathbf{r}_{\scriptscriptstyle SB}\|_2^2}$ and $\beta_{\scriptscriptstyle SB}^{\scriptscriptstyle DB}=\frac{\alpha_{\scriptscriptstyle TX}}{\|\mathbf{r}_{\scriptscriptstyle SB}\|_2\|_2\|\mathbf{r}_{\scriptscriptstyle SB}-\mathbf{r}_{\scriptscriptstyle DB}\|_2\|\mathbf{r}_{\scriptscriptstyle DB}\|_2}$ are the combined scaling for single- and double-bounce due to the per-element transmit gain $\alpha_{\scriptscriptstyle TX}$ and the inverse-distance propagation path loss. The terms $f_{\scriptscriptstyle D}^{\scriptscriptstyle SB}$ and $f_{\scriptscriptstyle D}^{\scriptscriptstyle DB}$ denote the single-bounce and double-bounce Doppler frequencies,

$$\begin{bmatrix} f_{\text{BB}}^{\text{SB}} \\ f_{\text{D}}^{\text{B}} \end{bmatrix} = \frac{f_{\text{c}}}{c} \begin{bmatrix} 2\bar{\mathbf{r}}_{\text{SB}}^{\top} \\ \bar{\mathbf{r}}_{\text{SB}}^{\top} + (\bar{\mathbf{r}}_{\text{SB}}^{\text{DB}})^{\top} \end{bmatrix} \mathbf{v}_{\text{SB}}, \tag{2}$$

proportional to projecting \mathbf{v}_{SB} onto unit vectors along single-and double-bounce paths, $\bar{\mathbf{r}}_{\text{SB}} = \frac{\mathbf{r}_{\text{SB}}}{\|\mathbf{r}_{\text{SB}}\|_2}$, $\bar{\mathbf{r}}_{\text{SB}}^{\text{DB}} = \frac{\mathbf{r}_{\text{SB}} - \mathbf{r}_{\text{DB}}}{\|\mathbf{r}_{\text{SB}} - \mathbf{r}_{\text{DB}}\|_2}$. The vector \mathbf{n} denotes additive noise, modeled as zero mean uncorrelated complex Gaussian with identity covariance.

2.2. Problem Statement

The radar aims to estimate the moving object's velocity vector \mathbf{v}_{SB} from measurements $\mathbf{y}(\omega; p)$, given prior static object location estimate $\hat{\mathbf{r}}_{DB}$ from background processing. We assume no prior knowledge of the moving object's location \mathbf{r}_{SB} .

3. PROPOSED APPROACH

We propose a three-stage procedure to solve the problem formulated in Section 2.2. First, the radar estimates the moving object's location \mathbf{r}_{SB} and Doppler frequency via *single-bounce* processing. Next, the radar estimates the Doppler frequency along the *double-bounce* path based on prior knowledge of the static object's location $\hat{\mathbf{r}}_{\text{DB}}$. Finally, the estimated single-bounce and double-bounce Doppler frequencies are used to estimate the moving object's velocity vector \mathbf{v}_{SB} .

Stage 1 (*Single-Bounce*): The radar first computes the following intermediate function for a hypothetical 2D location in the environment \mathbf{r} and chirp index \mathbf{p} :

$$\hat{\sigma}_{\mathbf{r}}^{SB}(\mathbf{p}) = \frac{1}{W} \sum_{\omega} \frac{e^{j\omega \frac{2\|\mathbf{r}\|_{2}}{c}}}{\beta_{SB}(\mathbf{r})} (\mathbf{a}_{RX}(\theta_{\mathbf{r}}) \otimes \mathbf{a}_{TX}(\theta_{\mathbf{r}}))^{\mathsf{H}} \mathbf{y}(\omega; \mathbf{p}), (3)$$

where $(\cdot)^H$ denotes the Hermitian operator, W is the number of instantaneous FMCW frequencies ω , and $\beta_{SB}(\mathbf{r}) = \frac{\alpha_{TX}}{\|\mathbf{r}\|_2^2}$. Intuitively, (3) is a matched filter along single-bounce paths to/from locations \mathbf{r} . The moving object's location \mathbf{r}_{SB} and single-bounce Doppler frequency are then estimated via:

$$\left(\hat{\mathbf{r}}_{SB}, \hat{\mathbf{f}}_{D}^{SB}\right) = \arg\max_{\mathbf{r}, \mathbf{f}_{D}} \left| \frac{1}{P} \sum_{\mathbf{p}} \hat{\sigma}_{\mathbf{r}}^{SB}(\mathbf{p}) e^{j2\pi \mathbf{f}_{D} \mathbf{p} \mathsf{T}_{c}} \right|^{2}, \quad (4)$$

which can be implemented with low complexity via IFFT³.

Stage 2 (*Double-Bounce*): Given location estimates of both objects, $\hat{\mathbf{r}}_{SB}$, $\hat{\mathbf{r}}_{DB}$, the double-bounce Doppler frequency is estimated via the double-bounce analogue of Stage 1:

$$\hat{\sigma}_{\mathbf{r}}^{\mathsf{DB}}(\mathsf{p}) = \frac{1}{\mathsf{W}} \sum_{\mathsf{M}} \frac{e^{j\frac{\omega}{\mathsf{c}}\mathsf{d}_{\mathsf{SB}}^{\mathsf{r}}}}{\beta_{\mathsf{SB}}^{\mathsf{DB}}(\hat{\mathbf{r}}_{\mathsf{SB}}; \mathbf{r})} (\tilde{\mathbf{a}}(\theta_{\mathbf{r}}, \hat{\theta}_{\mathsf{SB}}))^{\mathsf{H}} \mathbf{y}(\omega; \mathsf{p}), \quad (5)$$

$$\hat{\mathbf{f}}_{D}^{DB} = \arg \max_{\mathbf{f}_{D}} \left| \frac{1}{P} \sum_{\mathbf{p}} \hat{\sigma}_{\mathbf{r} = \hat{\mathbf{r}}_{DB}}^{DB}(\mathbf{p}) e^{j2\pi f_{D} \mathbf{p} T_{c}} \right|^{2}, \quad (6)$$

where $eta_{\scriptscriptstyle{\mathsf{SB}}}^{\scriptscriptstyle{\mathsf{DB}}}(\hat{\mathbf{r}}_{\scriptscriptstyle{\mathsf{SB}}};\mathbf{r}) = \frac{\alpha_{\scriptscriptstyle{\mathsf{TX}}}}{\|\hat{\mathbf{r}}_{\scriptscriptstyle{\mathsf{SB}}}\|_2 \|\hat{\mathbf{r}}_{\scriptscriptstyle{\mathsf{SB}}} - \mathbf{r}\|_2 \|\mathbf{r}\|_2}, \, \mathbf{d}_{\scriptscriptstyle{\mathsf{SB}}}^{\mathbf{r}} = \|\hat{\mathbf{r}}_{\scriptscriptstyle{\mathsf{SB}}}\|_2 + \|\hat{\mathbf{r}}_{\scriptscriptstyle{\mathsf{SB}}} - \mathbf{r}\|_2 + \|\mathbf{r}\|_2, \, \tilde{\mathbf{a}}(\theta_{\mathbf{r}}, \hat{\theta}_{\scriptscriptstyle{\mathsf{SB}}}) = \mathbf{a}_{\scriptscriptstyle{\mathsf{RX}}}(\theta_{\mathbf{r}}) \otimes \mathbf{a}_{\scriptscriptstyle{\mathsf{TX}}}(\hat{\theta}_{\scriptscriptstyle{\mathsf{SB}}}) + \mathbf{a}_{\scriptscriptstyle{\mathsf{RX}}}(\hat{\theta}_{\scriptscriptstyle{\mathsf{SB}}}) \otimes \mathbf{a}_{\scriptscriptstyle{\mathsf{TX}}}(\theta_{\mathbf{r}}), \, \\ \text{and } \hat{\theta}_{\scriptscriptstyle{\mathsf{SB}}} \text{ is the azimuth angle of the location estimate } \hat{\mathbf{r}}_{\scriptscriptstyle{\mathsf{SB}}}.$

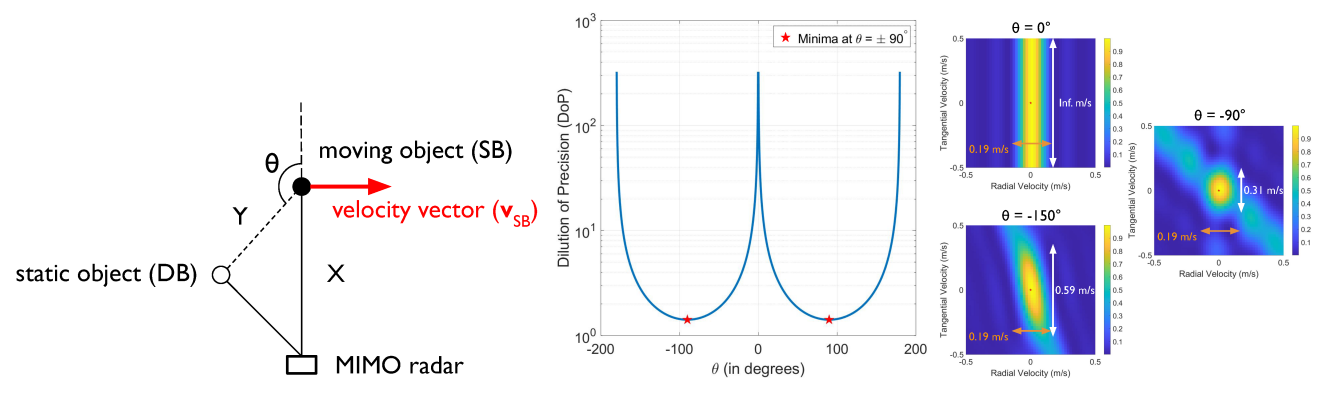
Stage 3 (*Velocity Estimation*): Finally, given estimates of the single-bounce and double-bounce Doppler frequencies, \hat{f}_D^{SB} and \hat{f}_D^{DB} , the velocity vector \mathbf{v}_{SB} is estimated as follows:

$$\hat{\mathbf{v}}_{\text{SB}} = \frac{c}{f_{c}} \begin{bmatrix} 2\bar{\hat{\mathbf{r}}}_{\text{SB}}^{\top} \\ \bar{\hat{\mathbf{r}}}_{\text{SR}}^{\top} + (\hat{\hat{\mathbf{r}}}_{\text{SB}}^{\text{DB}})^{\top} \end{bmatrix}^{\dagger} \begin{bmatrix} \hat{\mathbf{f}}_{\text{SB}}^{\text{SB}} \\ \hat{\mathbf{f}}_{\text{D}}^{\text{BB}} \end{bmatrix}, \tag{7}$$

¹relative to the radar's location (assumed at origin of coordinate system)

²frequency-modulated continuous wave

³inverse fast Fourier transform



- (a) Simulated configuration and notation.
- (b) Dilution of precision vs angle θ . (c) Ambiguity function for different θ .

Fig. 2: (a) Key notation used in simulations. (b) Dilution of precision (DoP) is minimum ("best"), with value $\sqrt{2}$, when $\theta = \pm 90^{\circ}$. (c) Tangential velocity resolution is smallest ("best") when $\theta = \pm 90^{\circ}$, and infinite ("worst") when $\theta = 0^{\circ}$, $\pm 180^{\circ}$.

where $(\cdot)^{\dagger}$ denotes the pseudo-inverse, and $\bar{\hat{\mathbf{r}}}_{\text{SB}}$ and $\bar{\hat{\mathbf{r}}}_{\text{SB}}^{\text{DB}}$ denote the unit vectors along the estimated single- and double-bounce paths, $\bar{\hat{\mathbf{r}}}_{\text{SB}} = \frac{\hat{\mathbf{r}}_{\text{SB}}}{\|\hat{\mathbf{r}}_{\text{SB}}\|_2}$ and $\bar{\hat{\mathbf{r}}}_{\text{SB}}^{\text{DB}} = \frac{\hat{\mathbf{r}}_{\text{SB}} - \hat{\mathbf{r}}_{\text{DB}}}{\|\hat{\mathbf{r}}_{\text{SB}} - \hat{\mathbf{r}}_{\text{DB}}\|_2}$. Note that the pseudo-inverse in (7) can be implemented with low complexity since the underlying matrix is of size 2×2 .

4. RESULTS

We present both analytical and simulation results to quantify the performance of the proposed approach. We begin by theoretically quantifying the impact of the system geometry – locations of the two objects – on the performance of the velocity vector estimator in (7), assuming perfect estimates $\hat{\mathbf{r}}_{\text{SB}},~\hat{\mathbf{r}}_{\text{DB}}$ and $\hat{f}_{\text{D}}^{\text{SB}},~\hat{f}_{\text{D}}^{\text{DB}}$ from Stages 1 and 2.

Lemma 1. Assuming perfect estimates from Stages 1 and 2, perfect estimation of the velocity vector \mathbf{v}_{SB} is possible via (7) as long as the moving and static objects are not collinear,

$$\mathbf{r}_{\text{DB}} \neq \alpha \mathbf{r}_{\text{SB}}, \ \forall \alpha.$$

Proof. Velocity vector \mathbf{v}_{SB} can be perfectly estimated if the 2×2 matrix in (2) has full rank. It is easy to see that this is the case if the unit vectors satisfy $\bar{\mathbf{r}}_{\text{SB}}^{\text{DB}} \neq \bar{\mathbf{r}}_{\text{SB}}$, which is equivalent to having non-collinear object locations $\mathbf{r}_{\text{DB}} \neq \alpha \mathbf{r}_{\text{SB}}$, $\forall \alpha$. \Box

While Lemma 1 suggests that any two non-collinear object locations \mathbf{r}_{SB} , \mathbf{r}_{DB} suffice to perfectly estimate the velocity vector \mathbf{v}_{SB} , the practical performance of the proposed approach depends on the properties of the pseudo-inverse estimate in (7). To quantify the performance of (7) as a function of the object locations \mathbf{r}_{SB} , \mathbf{r}_{DB} , we adapt the well-known notion of the *dilution of precision* (DoP) to our system.

Definition 1 ([12]). Consider a linear system y = Ax + n, with zero mean uncorrelated noise vector n with identity covariance. Let \hat{x} denote the pseudo-inverse solution for x,

i.e., $\hat{\mathbf{x}} = \mathbf{A}^{\dagger}\mathbf{y}$. The dilution of precision (DoP) is defined as the square root of the trace of the covariance of $\hat{\mathbf{x}}$,

$$\mathsf{DoP} = \sqrt{\mathsf{Tr} \bigg[\mathsf{cov}(\hat{\mathbf{x}}) \bigg]} = \sqrt{\mathsf{Tr} \bigg[\big(\mathbf{A}^{\top} \mathbf{A} \big)^{-1} \bigg]}.$$

In the context of our system, the matrix **A** in Definition 1 corresponds to the matrix in (2), assuming perfect estimates $\hat{\bf r}_{_{SB}},~\hat{\bf r}_{_{DB}}$ and $\hat{\bf f}_{_D}^{_{SB}},~\hat{\bf f}_{_D}^{_{DB}}$ in (7) from Stages 1 and 2. To understand the variation of the DoP as a function of object locations \mathbf{r}_{SB} , \mathbf{r}_{DB} , we simulate the configuration shown in Fig. 2(a), with the static object oriented at an angle θ with respect to the radar's line-of-sight, where the moving object is located. Note that the precise values of the object locations \mathbf{r}_{SB} , \mathbf{r}_{DB} are not important since the DoP only depends on the unit vectors $\bar{\mathbf{r}}_{SB}$, $\bar{\mathbf{r}}_{DB}$. Fig. 2(b) shows the variation of the DoP as a function of angle θ , with smaller values of DoP considered "better" [12]. We observe that the DoP peaks to infinity at $\theta = 0^{\circ}$ and $\pm 180^{\circ}$, corresponding to static object locations that are collinear with the moving object. On the other hand, the DoP is minimum (with value $\sqrt{2}$) at $\theta=\pm 90^\circ$, corresponding to perpendicular unit vectors $\bar{\bf r}_{\rm SB} \perp \bar{\bf r}_{\rm SB}^{\rm DB}$, which is the most favorable geometry for velocity vector estimation.

To further quantify the performance gains in velocity vector estimation with our approach, we characterize the velocity *ambiguity function* [13]. Recall that all processing steps in (3)-(6) correspond to spatial and temporal *matched filters*. We thus define the velocity ambiguity function as the intensity of the coherent sum of all matched filter outputs:

$$\chi(\mathbf{v}; \mathbf{v}_{\mathrm{SB}}) = \left| \frac{1}{\mathsf{P}} \sum_{\mathbf{p}} \left[\hat{\sigma}_{\mathbf{r}_{\mathrm{SB}}}^{\mathrm{SB}}(\mathbf{p}) e^{j2\pi \mathbf{f}_{\mathrm{D}}^{\mathrm{SB}}(\mathbf{v})\mathbf{p}\mathsf{T}_{\mathrm{c}}} + \hat{\sigma}_{\mathbf{r}_{\mathrm{DB}}}^{\mathrm{DB}}(\mathbf{p}) e^{j2\pi \mathbf{f}_{\mathrm{D}}^{\mathrm{DB}}(\mathbf{v})\mathbf{p}\mathsf{T}_{\mathrm{c}}} \right] \right|^{2},$$

where we have assumed known object locations \mathbf{r}_{SB} , \mathbf{r}_{DB} . Variables $\hat{\sigma}_{\mathbf{r}}^{\text{S/DB}}(p)$, defined in (3) and (5), correspond to a ground-truth velocity vector \mathbf{v}_{SB} . Terms $f_{\text{D}}^{\text{SB}}(\mathbf{v}) = \frac{f_c}{c} 2 \langle \bar{\mathbf{r}}_{\text{SB}}, \mathbf{v} \rangle$ and $f_{\text{D}}^{\text{DB}}(\mathbf{v}) = \frac{f_c}{c} \langle \bar{\mathbf{r}}_{\text{SB}} + \bar{\mathbf{r}}_{\text{SB}}^{\text{DB}}, \mathbf{v} \rangle$ are Doppler frequencies for a

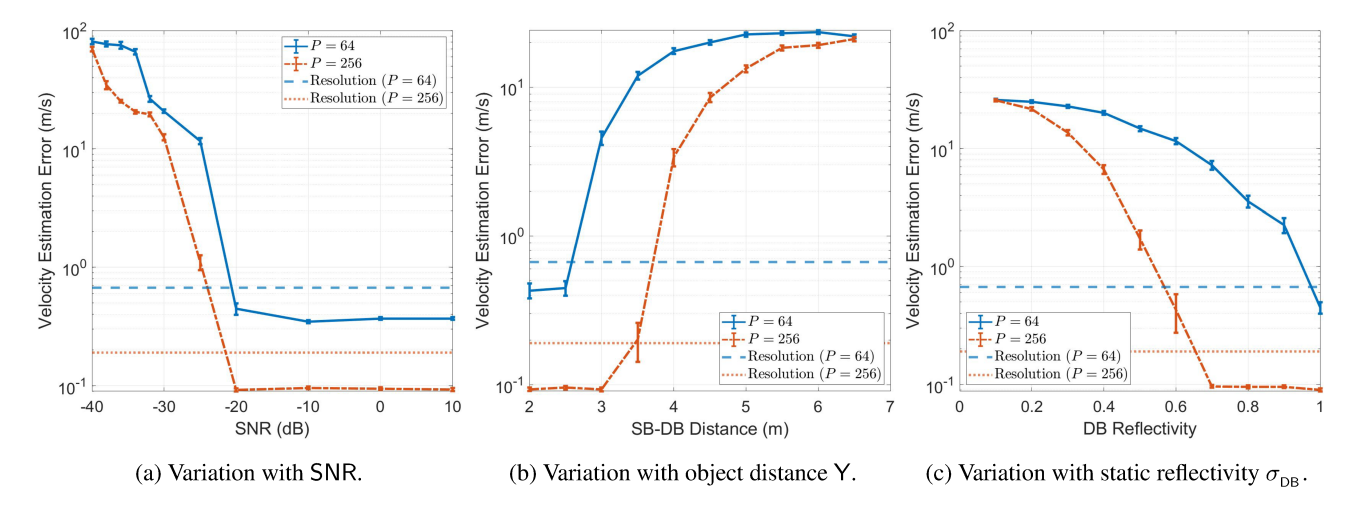


Fig. 3: (a) At low SNRs, noise prevents accurate velocity vector estimation. (b) Larger distances Y reduce double-bounce path power & increase estimation error. (c) Larger reflectivities σ_{DB} increase double-bounce path power & reduce estimation error.

hypothetical velocity vector \mathbf{v} . Intuitively, $\chi(\mathbf{v}; \mathbf{v}_{SB})$ should peak at $\mathbf{v} = \mathbf{v}_{SB}$ and decay elsewhere, with its half-power beamwidth denoting the system's velocity vector resolution.

Fig. 2(c) plots $\chi(\mathbf{v}; \mathbf{0})$ for three different values of angle $\theta \in \{0^{\circ}, -150^{\circ}, -90^{\circ}\}$ in Fig. 2(a), with unit-reflectivity objects at $\|\mathbf{r}_{\text{SB}}\|_2 = \mathsf{X} = 2.5$ m and $\|\mathbf{r}_{\text{SB}} - \mathbf{r}_{\text{DB}}\|_2 = \mathsf{Y} = 2.5$ m. The simulation parameters correspond to a commercial automotive millimeter-wave MIMO radar [14]: FMCW starting frequency $\mathsf{f}_{\mathsf{c}} = 77$ GHz, 4 GHz bandwidth with $\mathsf{W} = 256$ instantaneous chirp frequencies, $\mathsf{P} = 256$ chirps of duration $\mathsf{T}_{\mathsf{c}} = 40\mu \mathsf{s}$, and $\mathsf{T} = 9$, $\mathsf{R} = 16$ elements (arranged linearly).

When $\theta=0^\circ$, which corresponds to collinear objects and hence *single-bounce*-only processing, the ambiguity function has a ridge-like shape with infinite tangential velocity resolution and Doppler-limited radial velocity resolution of 0.19 m/s, thus verifying Lemma 1 and the DoP result from Fig. 2(b). The tangential velocity resolution is smallest when $\theta=-90^\circ$ (0.31 m/s), and spans the range $[0.31,\infty)$ m/s for intermediate values of θ , which is consistent with Fig. 2(b).

Next, we characterize the impact of noise on the end-to-end performance, quantified via the velocity estimation error, $\|\hat{\mathbf{v}}_{\text{SB}} - \mathbf{v}_{\text{SB}}\|_2$. Expressing the system model in (1) as $\mathbf{y}(\omega;\mathbf{p}) = \mathbf{s}(\omega;\mathbf{p}) + \mathbf{n}$, we define the signal-to-noise ratio (SNR) as SNR = $\frac{1}{\text{TRWP}} \sum_{\omega} \sum_{\mathbf{p}} \|\mathbf{s}(\omega;\mathbf{p})\|_2^2$, assuming the noise is zero mean with identity covariance. The SNR is thus a function of the transmit gain α_{TX} , reflectivities σ_{SB} , σ_{DB} and distances X, Y. In the following results, we assume $\theta = 90^\circ$ with a tangential velocity vector $\mathbf{v}_{\text{SB}} = \begin{bmatrix} v_{\text{SB}} & 0 \end{bmatrix}^\top$, and background subtraction of static object single-bounce returns.

In Fig. 3, we plot the mean velocity estimation error (with error bars showing the standard error of the mean) as a function of different system parameters, across 500 independent realizations of noise and tangential velocity $v_{\rm SB}$ uniformly distributed in [-5,5] m/s. Fig. 3(a) plots the velocity estimation error as a function of SNR by varying the transmit gain $\alpha_{\rm TX}$.

We observe a phase transition at an SNR threshold of -20 dB, beyond which the velocity estimation error drops to subresolution values and saturates. The reason for the phase transition is simple: at low SNRs, noise overwhelms Stages 1 and 2 of the proposed approach, preventing accurate moving object location and Doppler estimation. At high SNRs, Doppler frequency estimation errors (due to finite number of chirps P) in Stages 1 and 2 are the primary performance bottleneck.

In Figs. 3(b)-(c), we vary the double-bounce path power by varying the object distance $\|\mathbf{r}_{\text{SB}} - \mathbf{r}_{\text{DB}}\|_2 = Y$, and static object reflectivity, σ_{DB} , with the transmit gain α_{TX} set to ensure -20 dB SNR at Y = 2.5 m. We observe that the errors exhibit phase transitions, e.g., beyond Y = 3 m and $\sigma_{\text{DB}} = 0.7$ for P = 256. Increasing distance Y and reducing reflectivity σ_{DB} reduces the double-bounce path power, which makes it challenging to estimate the double-bounce Doppler frequency in Stage 2 and results in larger estimation errors. The trends for P = 64 are similar but with larger errors and thresholds, consistent with the findings in Fig. 3(a).

5. CONCLUDING REMARKS

In this paper, we proposed to exploit double-bounce scattering from a static object to estimate the entire velocity vector of a moving object with a MIMO radar. The key insight is that double-bounce paths carry information about tangential velocity components, which can be estimated by jointly processing the single-bounce and double-bounce paths. In future work, we will explore extensions to multiple static and moving objects (both point-like and extended), different multibounce orders (triple-bounce and beyond), multiple radars, and consider the problem of designing and placing dedicated reflectors to enable on-car radars to estimate the velocity vectors of other vehicles and pedestrians. We also plan to validate all results with real-world experimental data.

6. REFERENCES

- [1] J. Gunnarsson, L. Svensson, L. Danielsson, and F. Bengtsson, "Tracking Vehicles using Radar Detections," in 2007 IEEE Intelligent Vehicles Symposium, 2007, pp. 296–302.
- [2] Christina Knill, Alexander Scheel, and Klaus Dietmayer, "A Direct Scattering Model for Tracking Vehicles with High-Resolution Radars," in 2016 IEEE Intelligent Vehicles Symposium (IV), 2016, pp. 298–303.
- [3] Edin Insanic and Paul R. Siqueira, "A Maximum Likelihood Approach to Estimation of Vector Velocity in Doppler Radar Networks," *IEEE Transactions on Geo*science and Remote Sensing, vol. 50, no. 2, pp. 553– 567, 2012.
- [4] Dominik Kellner, Michael Barjenbruch, Jens Klappstein, Jürgen Dickmann, and Klaus Dietmayer, "Instantaneous Full-Motion Estimation of Arbitrary Objects using Dual Doppler Radar," in 2014 IEEE Intelligent Vehicles Symposium Proceedings, 2014, pp. 324–329.
- [5] Stefan Edstaller and Dominik Mueller, "A Cooperative Radar System With Active Reference Target Synchronization for Kinematic Target Analysis," *IEEE Transactions on Microwave Theory and Techniques*, vol. 69, no. 9, pp. 4118–4131, 2021.
- [6] Seung-Gu Lee, Jaehoon Jung, and Seong-Cheol Kim, "Enhanced Velocity Vector Estimation Using Distributed Radar System," in 2022 IEEE VTS Asia Pacific Wireless Communications Symposium (APWCS), 2022, pp. 75–79.
- [7] Johannes Schlichenmaier, Maximilian Steiner, Timo Grebner, and Christian Waldschmidt, "Clustering and

- Subsequent Contour and Motion Estimation of Automotive Objects Using a Network of Cooperative Radar Sensors," *IEEE Transactions on Vehicular Technology*, vol. 72, no. 1, pp. 428–443, 2023.
- [8] Yunfei Long, Daniel Morris, Xiaoming Liu, Marcos Castro, Punarjay Chakravarty, and Praveen Narayanan, "Full-Velocity Radar Returns by Radar-Camera Fusion," in *Proceedings of the IEEE/CVF International Conference on Computer Vision (ICCV)*, October 2021, pp. 16198–16207.
- [9] Dominik Kellner, Michael Barjenbruch, Klaus Dietmayer, Jens Klappstein, and Jürgen Dickmann, "Instantaneous Lateral Velocity Estimation of a Vehicle using Doppler Radar," in *Proceedings of the 16th International Conference on Information Fusion*, 2013, pp. 877–884.
- [10] Johannes Schlichenmaier, Leping Yan, Martin Stolz, and Christian Waldschmidt, "Instantaneous Actual Motion Estimation with a Single High-Resolution Radar Sensor," in 2018 IEEE MTT-S International Conference on Microwaves for Intelligent Mobility (ICMIM), 2018, pp. 1–4.
- [11] Nihal Singh, Dibakar Sil, and Ankit Sharma, "Parallelized Instantaneous Velocity and Heading Estimation of Objects using Single Imaging Radar," in 2021 IEEE Radar Conference (RadarConf21), 2021, pp. 1–6.
- [12] Richard B Langley et al., "Dilution of Precision," *GPS World*, vol. 10, no. 5, pp. 52–59, 1999.
- [13] Geoffrey San Antonio, Daniel R. Fuhrmann, and Frank C. Robey, "MIMO Radar Ambiguity Functions," *IEEE Journal of Selected Topics in Signal Processing*, vol. 1, no. 1, pp. 167–177, 2007.
- [14] Texas Instruments, "AWR2243 Four-Chip Cascade mmWave Radar," 2019.